JOURNAL OF GEOPHYSICAL RESEARCH, VOL. 112, D10S22, doi:10.1029/2006JD007605, 2007

Aerosol acidity in rural New England: Temporal trends and source region analysis

L. D. Ziemba,[1,2] E. Fischer,[1,2,3,4] R. J. Griffin,[1,2] and R. W. Talbot[1]

Received 31 May 2006; revised 27 November 2006; accepted 9 January 2007; published 26 April 2007.

[1] Data from 24-hour bulk filter samples collected by the AIRMAP program were used to estimate aerosol acidity at a site in New England. The sampling site, Thompson Farm in Durham, New Hampshire, is situated 15 km inland from the Atlantic Ocean. The aerosol chemical composition in this area is dominated by sulfate (SO_4^{2-}) and ammonium (NH_4^+) and aerosols that are weakly acidic, most likely because of a lack of regional sources of gaseous ammonia (NH_3). Nitrate (NO_3^-) plays a smaller role in aerosol acidity. The median SO_4^{2-} aerosol concentration was highest during the summer (23.7 nmol m^{-3}). Inferred fine NO_3^- concentrations were highest in the winter, with a median concentration of 0.2 nmol m^{-3}. Increased inferred hydrogen ion concentrations and the least neutralized aerosols are associated most strongly with coastal sources, potentially because of smaller NH_3 sources relative to sulfur sources in these regions. During the International Consortium for Atmospheric Research on Transport and Transformation (ICARTT) campaign during summer 2004, the composition of fine aerosol was dominated by SO_4^{2-}, NH_4^+, and organics. Acidic aerosols sampled during this campaign were largely anthropogenic in origin and photochemically aged.

Citation: Ziemba, L. D., E. Fischer, R. J. Griffin, and R. W. Talbot (2007), Aerosol acidity in rural New England: Temporal trends and source region analysis, *J. Geophys. Res.*, *112*, D10S22, doi:10.1029/2006JD007605.

1. Introduction

[2] Atmospheric aerosols exert influences on global climate [*Charlson et al.*, 1992a], biogeochemical cycling [*Charlson et al.*, 1992b], visibility [*Dzubay et al.*, 1982], and human health [*Spengler et al.*, 1990; *Schlesinger and Cassee*, 2003]. Primary emission of aerosols is a significant contributor by mass to atmospheric particulate matter (PM). Just as significant are secondary processes such as oxidation, condensation, coagulation, and neutralization that greatly affect the chemical composition and size distribution of aerosols. Considerable work in the last 50 years has focused on quantifying the size-resolved chemical composition of aerosols to understand better the processes that influence the chemistry of the atmosphere.

[3] Sulfate (SO_4^{2-}) is a major constituent of atmospheric aerosol and has a trimodal distribution across the submicron and supermicron size spectrum [*Wall et al.*, 1988]. Fine aerosol (here defined as aerosol with diameters less than 2.5 μm, though also defined in some contexts on the basis of 1 μm) SO_4^{2-} originates partially from the dissociation of sulfuric acid (H_2SO_4) that condenses after forming via the gas phase oxidation of sulfur dioxide (SO_2) by hydroxyl radical (OH). It may also exist as a result of the formation of salts of H_2SO_4 [*Stockwell and Calvert*, 1983]. Aqueous phase oxidation of SO_2 by hydrogen peroxide (H_2O_2) [*Kunen et al.*, 1983] or ozone (O_3) [*Botha et al.*, 1994] also contributes to fine SO_4^{2-}. Sulfur dioxide is emitted primarily from the burning of fossil fuels. Additional sources of reduced sulfur compounds that contribute to aerosol SO_4^{2-} after being oxidized include the ocean (dimethyl sulfide and carbonyl sulfide) [*Fitzgerald*, 1991], wetlands and soils [*Charlson et al.*, 1992b], and volcanic eruptions (hydrogen sulfide) [*Bluth et al.*, 1994]. Aerosol SO_4^{2-} exists in the coarse mode (aerosol with diameters greater than 2.5 μm) primarily through displacement reactions, mainly in mineral dust [*Li-Jones and Prospero*, 1998] and sea-salt aerosol [*McInnes et al.*, 1994].

[4] Nitrate (NO_3^-) is another major chemical constituent of atmospheric aerosols. Nitrate arises in the fine mode because of the dynamic equilibrium of ammonium nitrate (NH_4NO_3) with nitric acid (HNO_3) and ammonia (NH_3) in the particle and gas phases, respectively. Nitric acid is formed from the oxidation of nitrogen oxides (NO_x) during the day and from hydrolysis of dinitrogen pentoxide (N_2O_5) at night. Dinitrogen pentoxide is formed in the reaction between the nitrate radical and nitrogen dioxide (NO_2). Nitrate also exists in the coarse aerosol mode [*Savoie and Prospero*, 1982] in sea-salt and mineral dust aerosol as a result of displacement reactions [*Gard et al.*, 1998; *Newberg et al.*, 2005].

[5] Ammonium (NH_4^+), which results in the aerosol phase through gas-to-aerosol conversion of NH_3, is an important

[1]Institute for the Study of Earth, Oceans, and Space, Climate Change Research Center, University of New Hampshire, Durham, New Hampshire, USA.
[2]Department of Earth Sciences, University of New Hampshire, Durham, New Hampshire, USA.
[3]Mount Washington Observatory, North Conway, New Hampshire, USA.
[4]Now at Department of Atmospheric Sciences, University of Washington, Seattle, Washington, USA.

0148-0227/07/2006JD007605$09.00

water-soluble component of fine ambient aerosol. Ammonia is emitted primarily from animal wastes, fertilizers, soils, and oceans [*Bouwman et al.*, 1997] and is the major basic gas both over the continents and in the marine atmosphere. As a result, NH_4^+ is the major neutralizing component of atmospheric aerosol.

[6] Depending on the relative concentrations of these ions (which vary on the basis of differing oxidation rates, oxidation processes, and emission rates of precursors), atmospheric aerosols may exhibit acidic properties [*Huntzicker et al.*, 1980]. Such aerosol acidity has been shown to influence aerosol phase reactions, catalyzing processes that result in increased yields of secondary organic aerosol (SOA) [*Jang et al.*, 2002; *Iinuma et al.*, 2004]. In addition, particle acidity is thought to play a role in health effects associated with poor air quality [*Spengler et al.*, 1990]. Therefore it is crucial to understand the acidity of particles and the factors that control it. Aerosol strong acidity has been studied previously, mostly during summer months, during shorter field campaigns, and in specific locations [*Smith-Palmer and Wentzell*, 1986; *Koutrakis et al.*, 1988; *Keeler et al.*, 1990; *Waldman et al.*, 1990; *U.S. Environmental Protection Agency* (*USEPA*), 1999; *Lefer and Talbot*, 2001]. Additional studies have focused on longer trends in a single ionic species such as SO_4^{2-} [*Malm et al.*, 2002].

[7] The northeastern United States is of particular interest with regard to acidic aerosol because of its downwind location relative to industrial areas in the midwestern United States and major metropolitan areas along the eastern seaboard of the United States. Previous work has shown that regional transport greatly affects the air quality of New England [*Knapp et al.*, 1998; *Schultz et al.*, 1998; *Fischer et al.*, 2004; *Mao and Talbot*, 2004a, 2004b]. The International Consortium for Atmospheric Research on Transport and Transformation (ICARTT) campaign was conducted during the summer of 2004 to increase the understanding of air quality parameters in North America and to understand how the long-range transport of pollution across the Atlantic Ocean affects air quality downwind [*Fehsenfeld et al.*, 2006]. As part of ICARTT, the National Oceanic and Atmospheric Administration–University of New Hampshire (NOAA-UNH) AIRMAP Cooperative Institute performed measurements of pollutant concentrations and meteorological data to document tropospheric air quality in the New England area.

[8] This paper discusses seasonal trends in the chemical composition and acidity of aerosols at the UNH Atmospheric Observatory at Thompson Farm (TF). A Lagrangian backward trajectory model has been used to understand source regions of aerosol transported to this site. Correlations between aerosol species and source regions are discussed on a seasonal basis, and year-to-year variations are investigated. A detailed discussion of size-segregated aerosol measurements, including those of carbonaceous material, made during ICARTT is also provided.

2. Methods

2.1. Field Site

[9] All data used in this study were collected in conjunction with the UNH-based AIRMAP program. This study involves data collected at the AIRMAP site at TF, located in Durham, New Hampshire, at 43.11°N, 70.95°W. This is a rural site situated approximately 15 km from the Atlantic Ocean and at 24 m above sea level. Sampling was performed at both 15 m and 4 m above ground level from a walk-up, instrumented tower.

2.2. Aerosol Sampling and Instrumentation

[10] Sampling of bulk aerosol (dating from January 2000 to November 2004) was used in this study to assess the chemical composition of aerosol at TF. Samples were collected over 24-hour time intervals on 90-mm Teflon® filters (Fluropore™, Millipore, Billerica, Massachusetts). An aerosol size cut of approximately 10 μm was estimated using sampling apparatus geometry, fluid dynamics, and an estimated inlet flow rate of 100 L min^{-1}. The exact aerosol size cut is affected by minor variations in flow rate. No denuders were employed during bulk filter sampling. The mass loadings of common inorganic ions (SO_4^{2-}, NO_3^-, NH_4^+, Na^+, Ca^{2+}, K^+, Mg^{2+}, and Cl^-) were determined quantitatively by ion chromatography (IC). Filters were extracted into a H_2O/methanol solution, preserved in chloroform to inhibit biologic activity, and analyzed by IC using previously reported procedures [*DeBell et al.*, 2004].

[11] Detection limits for K^+, Mg^{2+}, Cl^-, and NO_3^- were determined on the basis of IC analysis because of their quantifiable presence in blank samples. The lowest quantifiable concentrations for these ions (based on concentrations in extraction water and assuming a 20-ml extraction volume and 24-hour sampling duration) are 0.010 nmol m^{-3} (K^+), 0.021 nmol m^{-3} (Mg^{2+}), 0.0062 nmol m^{-3} (Cl^-), and 0.021 nmol m^{-3} (NO_3^-). The uncertainty in the measurement of each of these species is calculated as three times the standard deviation of blank and duplicate samples and is reported as follows: 0.07 nmol m^{-3} (K^+), 0.17 nmol m^{-3} (Mg^{2+}), 0.50 nmol m^{-3} (Cl^-), and 0.17 nmol m^{-3} (NO_3^-). Because SO_4^{2-}, NH_4^+, Na^+, and Ca^{2+} were not present at quantifiable levels in blank samples, detection limits for these species are equal to the measurement uncertainty (computed as three times the standard deviation of duplicate samples) and are as follows: 0.30 nmol m^{-3} (SO_4^{2-}), 0.51 nmol m^{-3} (NH_4^+), 0.69 nmol m^{-3} (Na^+), and 0.12 nmol m^{-3} (Ca^{2+}).

[12] A Versatile Air Pollutant Sampler (VAPS, University Research Glass, URG, Chapel Hill, North Carolina) was employed for 3 weeks during the ICARTT campaign to assess the distribution of chemical components between the fine and coarse aerosol size modes and to determine the organic carbon (OC) and elemental carbon (EC) concentrations of fine aerosol. The VAPS used a cyclone to remove PM larger than 10 μm in aerodynamic diameter. A virtual impactor separated the sample flow into three trains, two of which sampled fine aerosol and one of which sampled coarse aerosol. One of the fine sampling trains was used for inorganic and gravimetric analysis, and the other was used for carbonaceous constituent analysis. The coarse aerosol samples were analyzed only for inorganic constituents and gravimetric mass loadings.

[13] The inorganic fine aerosol sampling train consisted of two annular denuders followed by a filter pack. The first denuder (URG, three-channel Teflon®-coated stainless steel, 242 mm in length) was coated with a citric acid solution to remove basic gases. This denuder was followed

directly by a second denuder (URG, three-channel Teflon®-coated stainless steel, 150 mm in length) that was coated with a sodium carbonate solution to remove acidic gases such as hydrochloric acid (HCl) and HNO_3. Following the denuders in series was a filter pack (URG, Teflon® coated). A Zefluor® membrane filter (47-mm diameter, 2-μm pore size, Pall Life Sciences, East Hills, New York) was supported by a Teflon®-coated porous screen inside the pack and collected the aerosol sample. Inorganic water-soluble ion concentrations were determined by IC using the same protocol as that used for the bulk filter analyses.

[14] Negative artifacts caused by evaporation of aerosol inorganic chemical constituents when employing denuders during filter sampling have been documented previously (for example, in the study of *Tsai and Perng* [1998]). Such artifacts should not apply to the bulk filter sampling in this study because no denuders were used; they are applicable to the VAPS samples, however. Significant losses of NO_3^- from denuded Teflon® filters (18–52%) were reported by *Yu et al.* [2005], with lost NO_3^- likely in the form of NH_4NO_3. Reported discrepancies between lost NH_4^+ and NO_3^- for denuded Teflon® filter samples could also indicate the presence of organic ammonium salts [*Yu et al.*, 2006]. Given the sampling and analysis techniques used here, it is not possible to address this possibility. Because of the range of NO_3^- losses reported above and the lack of necessary information, no effort is made here to correct for evaporative losses of NO_3^-. Sulfate aerosol is less prone to evaporation on filters due to low vapor pressure.

[15] The organic fine aerosol sampling train consisted of only a filter pack (URG, Teflon® coated) with no denuder. A prefired, quartz-fiber filter (47-mm diameter Pallflex® Tissuquartz, Pall Life Sciences, East Hills, New York) was used in this pack to collect aerosol samples to be analyzed for carbonaceous constituents. The concentrations of OC and EC were determined by a thermo-optical technique [*Birch and Cary*, 1996] by Sunset Laboratory, Inc. (Hillsborough, North Carolina). A factor of 1.4 has been used to convert the mass of OC (in carbon mass units) to total organic mass (OM) [*Russell*, 2003] although values of up to 2.1 have been reported previously [*Turpin and Lim*, 2001]. The range of values of the OM to OC ratio affects closure between gravimetric mass and calculated chemical species mass but has a negligible effect on relative values of the OM to SO_4^{2-} ratio discussed later in this manuscript.

[16] Positive artifacts that may have arisen from the lack of denudation of carbonaceous aerosol samples were accounted for by applying a constant reduction of 0.5 μg C m^{-3} to each 24-hour sample based on *Subramanian et al.* [2004]. Negative artifacts are considered negligible because no denuder was used to upset gas/particle equilibrium. The coarse aerosol sampling train also consisted of only a filter pack (URG, Teflon® coated) loaded with a Zefluor® membrane filter (47-mm diameter, 2-μm pore size, Pall Life Sciences).

[17] Flow rates through each of the sampling trains were regulated by a pump and mass flow controller. The virtual impactor required fine aerosol train flow rates of 15 L min^{-1} and a coarse aerosol train flow rate of 2 L min^{-1} to achieve an accurate size cut, per manufacturer recommendations. The VAPS was housed in an insulated box that incorporated a thermostat, a heater, and a fan to maintain an internal temperature within ±4°C of the ambient temperature. Flow rates were calibrated several times during the sampling period using a standard Gilibrator (Gilian, Clearwater, Florida). Twenty-four-hour samples were taken daily for 3 weeks (28 July through 17 August 2004) from approximately 1000 to 1000 local time (EDT). All filters were sealed, wrapped in aluminum foil, and stored at 0°–10°C until analysis.

[18] Samples collected on Zefluor® filters were weighed to determine gravimetric mass loadings. Filters were pretreated by exposure (for 24 hours prior to sampling) to an aerosol-free environment that was stable with respect to temperature and humidity, per the method recommended by *USEPA* [2001]. The filters were then weighed and transported directly to the field site. Sampling occurred for 24 hours and was followed by a postsampling treatment in the same aerosol-free environment. The final aerosol mass was determined by the difference between presampling and postsampling filter mass.

2.3. Aerosol Acidity

[19] The acidity of atmospheric aerosols, which can be measured or estimated by several methods, is influenced mainly by SO_4^{2-}, NO_3^-, and NH_4^+ in the fine size mode. Oxidized sulfur exists as SO_4^{2-}, bisulfate ion (HSO_4^-), and H_2SO_4 [*Brosset*, 1978; *Charlson et al.*, 1978]. Sulfate exists almost exclusively in fine mode aerosol in the northeastern United States [*Lefer and Talbot*, 2001]. Using a ratio method similar to that of *Newberg et al.* [2005], all SO_4^{2-} in this study is assumed to be in the fine mode because the median fraction of sea-salt-derived SO_4^{2-} was very low: 2.0% based on the seawater SO_4^{2-} to Mg^{2+} mass ratio and 1.5% based on the seawater SO_4^{2-} to Na^+ mass ratio. In addition, less than 14% of backward trajectories (discussed subsequently) that reached TF passed directly over the ocean, limiting the likelihood of coarse SO_4^{2-} from displacement reactions.

[20] Nitrate aerosol, which is in dynamic equilibrium with HNO_3 in the fine mode, also occurs significantly in the coarse size modes in this area [*Jordan et al.*, 2000] mostly in the form of $CaNO_3$ and $NaNO_3$. Because our non-VAPS samples represent bulk aerosols, the distribution of fine and coarse mode NO_3^- must be estimated from the chemical analysis to properly assess the acidity of fine mode aerosol. Unlike SO_4^{2-}, it has been assumed that NO_3^- exists in the coarse size mode only through the displacement of chloride ion (Cl^-) in sea salt aerosol [*Wu and Okada*, 1994]. Occasionally, NO_3^- can be associated with coarse soil aerosol, but given low concentrations of total NO_3^- and soil constituents (Ca^{2+}, for example, with a median concentration of 1.36 nmol m^{-3}) at TF, these forms were assumed to be negligible. By subtracting the measured Cl^- concentration from that predicted based on the known ratio of Na^+ to Cl^- in seawater (0.55 by mass) and assuming all negative deviations are due to NO_3^- displacement, a coarse mode NO_3^- concentration was calculated (similar to the technique used by *Newberg et al.* [2005]). The concentration of fine NO_3^- was then calculated assuming a mass balance. Several instances occurred during the winter when the Cl^- concentration was in excess (though within measurement uncertainty) of that predicted using Na^+; this phenomenon was assumed to be associated with application of road salt on the

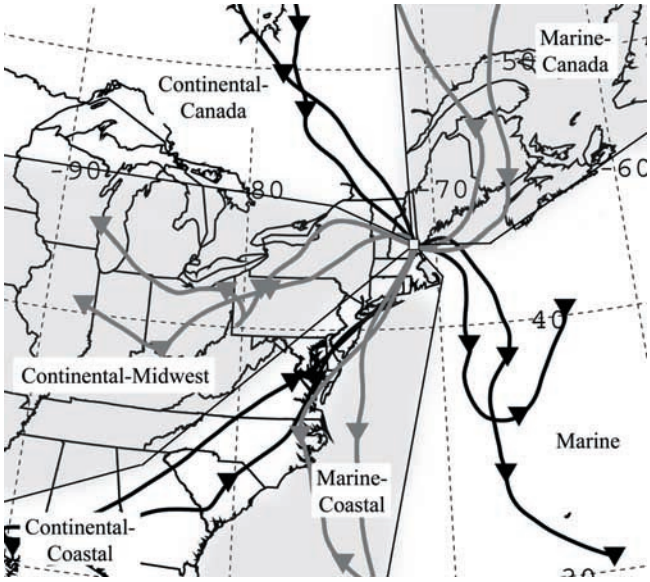

Figure 1. Example backward trajectories illustrating the source region classification scheme used for backward trajectory analyses. Two trajectories are plotted for each source region. Continental-Canada, marine, and continental coastal backward trajectories are shown in black; continental-midwest, marine-Canada, and marine-coastal are shown in gray. Backward trajectories are marked every 24 hours from the time of initialization with a triangle. All backward trajectories originate at TF, shown with a white square. Marine, marine-coastal, and continental-midwest regions are shaded in gray for to illustrate general areas of extent. Trajectories may have crossed regional boundaries slightly, but the areas of influence remain consistent each source region.

roads surrounding TF following snow storms. In addition, there were occasions when the predicted coarse NO_3^- concentration was slightly greater than the total concentration measured on the bulk filters (again generally within uncertainty). For these cases, it was assumed that all of the measured NO_3^- was distributed into the coarse mode and that the fine NO_3^- concentration was zero. All references to NO_3^- in the remainder of this paper refer to calculated fine NO_3^-.

[21] Assuming that SO_4^{2-}, NO_3^-, and NH_4^+ alone control fine aerosol acidity, an ion balance method was employed to approximate the relative aerosol acidity, or the concentration of hydrogen ion (H^+), in the aerosol phase [*Kerminen et al.*, 2001; *Schwab et al.*, 2004]. The concentration of H^+ was approximated by:

$$[H^+] = 2[SO_4^{2-}] + [NO_3^-] - [NH_4^+] \quad (1)$$

where the brackets imply ion concentrations, here in molar units. *Schwab et al.* [2004] discuss the applicability and limitations associated with this technique. This cation/anion balance assumes that the only unmeasured cation is H^+.

[22] The extent to which acidic aerosol is neutralized can also be approximated. Because the major gaseous base found in significant concentrations in the troposphere is NH_3, a ratio of inferred $[H^+]$ to the total concentration of cations can be used as a metric for acid purity, f, in the fine aerosol mode [*Stevens et al.*, 1980]:

$$f = \frac{[H^+]}{[H^+] + [NH_4^+]} = 1 - \frac{[NH_4^+]}{2[SO_4^{2-}] + [NO_3^-]} \quad (2)$$

Therefore f has values between zero and unity. If f is zero, every mole of SO_4^{2-} and NO_3^- has been neutralized fully by NH_4^+. If f is unity, no neutralization has occurred, and SO_4^{2-} and NO_3^- likely result from H_2SO_4 and HNO_3, respectively. At $f = 0.5$, the bulk aerosol exists as a mixture of chemical species and exhibits the properties of NH_4HSO_4; at $f = 0.25$, the mixture is similar to letovicite.

[23] While it is acknowledged fully that true aerosol acidity cannot be rigorously captured using these methods, it is satisfactory for longer timescales and seasonal trends. More robust techniques to calculate aerosol acidity that have been published previously utilize phase partitioning of soluble gases in addition to aerosol mass concentrations [*Keene et al.*, 2004]. However, such a method cannot be used in the current study because of lack of gas phase measurements of HNO_3 and NH_3.

2.4. Backward Trajectory Identification of Source Regions

[24] A Lagrangian transport model, the Hybrid Single-Particle Lagrangian Integrated Trajectory (HYSPLIT) model [*Draxler and Rolph*, 2003], has been used to understand air mass origin and thus to investigate the history of acidic aerosol arriving at TF. Three trajectories were computed for each 24-hour bulk filter sample, one each at 1200, 2000, and 0400 local time, to represent the 24-hour filter sample. Each trajectory was run for 72 hours, a standard calculation duration that should best describe relevant transport characteristics to the site. Trajectories were computed with a starting height of 750 m above sea level to minimize the number of backward trajectories that interacted with the model ground level. This elevation is well within the daytime boundary layer at this location. The archived Eta Data Assimilation System (EDAS) grid was used for meteorological input. The EDAS grid covers the continental United States and has a horizontal resolution of about 80 km and a vertical resolution of 22 pressure surfaces between 1000 and 50 hPa. The 80-km EDAS archive grid was only available through April 2004; thus, starting in May 2004, trajectories were run using the EDAS 40-km archive grid that replaced the 80-km grid. This grid has a horizontal resolution of about 40 km and a vertical resolution of 26 pressure surfaces between 1000 and 50 hPa.

[25] The trajectories associated with each sample were classified into the following general source regions: continental-Canada, continental-midwest, continental-coastal, marine-coastal, marine-Canada, and marine. Twelve example backward trajectories, two from each source region, are shown in Figure 1 to illustrate the classification scheme. Backward trajectories were sorted into these six source regions on the basis of visual inspection of the full path of each trajectory, and classification was independent of the associated vertical transport. While the continental-coastal and marine-coastal source regions may be indistinguishable from one another as they approach TF, the separation was

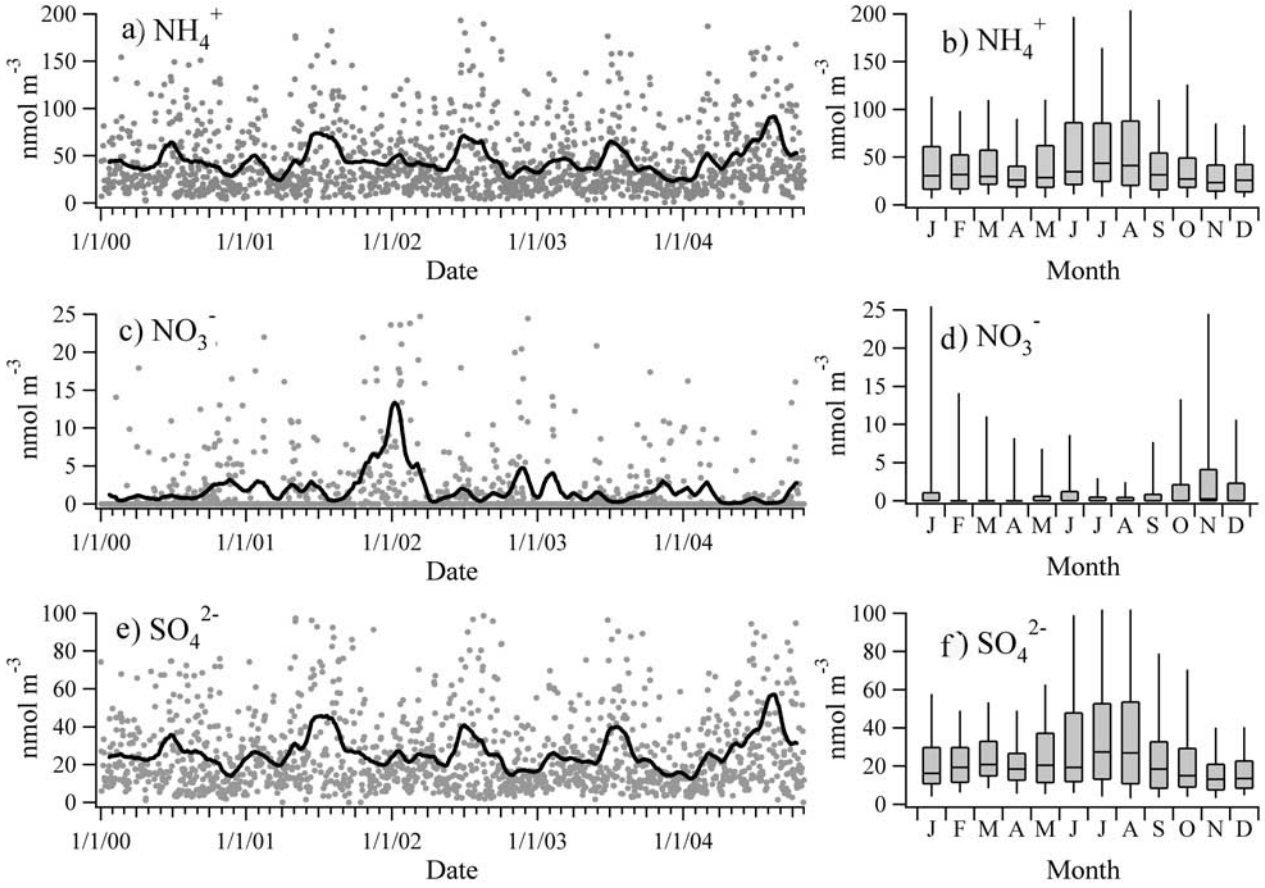

Figure 2. Time series and box plot analyses for (a and b) $[NH_4^+]$, (c and d) $[NO_3^-]$, and (e and f) $[SO_4^{2-}]$. A 30-day running average has been applied to each time series plot and is shown as a bold line. Box plot statistics are as follows: Median concentrations are represented by the line inside each box; the top and bottom of each box represents the 75th and 25th percentile values, respectively; and the top and bottom of each whisker represent the 95th and 5th percentile values, respectively.

made to differentiate between air masses that traveled up the coast but had very different longer-range sources further up stream.

[26] The maximum straight-line distance one trajectory traveled during all 72-hour runs to TF was approximately 4000 km, and the minimum distance traveled was approximately 600 km, a range of 3400 km. Backward trajectories classified as continental-Canada traveled the longest distances to TF, ranging from 4000 km to 1100 km. Continental-midwest backward trajectories had a similar maximum and minimum (3700 km, 700 km). The maximum and minimum straight-line distances for other source regions were considerably smaller, indicating slower moving air masses: 1700 km and 600 km in the marine region, 2300 km and 800 km in the continental-coastal region, 2600 km and 1000 km in the marine-coastal region, and 2700 km and 800 km in the marine-Canada region. Large ranges in the maximum and minimum distance traveled by backward trajectories within source regions could create a bias in chemistry between air masses, with faster moving air masses being subject to different emissions scenarios than slower moving air masses. However, this is expected to affect absolute aerosol concentrations to a greater extent than the general types (acidic versus nonacidic, biogenic versus anthropogenic, etc.) of aerosols observed within a given region.

[27] Trajectories were then grouped by the number of matching source regions per day. All further analysis was done only on data from filter samples that were associated with days characterized by two out of three consecutive matching backward trajectories for each day. In this way, mixing of different types of emissions sources was avoided. Air masses associated with very fast moving fronts and highly variable meteorological conditions (implying large changes in wind direction) thus have been ignored by this method.

3. Results

3.1. Seasonal Trends

[28] The time series of aerosol $[NH_4^+]$, $[NO_3^-]$, and $[SO_4^{2-}]$ are presented in Figures 2a, 2c, and 2e. Statistics for $[NH_4^+]$, $[NO_3^-]$, and $[SO_4^{2-}]$ are also presented in Tables 1–3, sorted by year and season. The aerosol inorganic composition is dominated by NH_4^+ and SO_4^{2-}, both on a molar (69% of the total moles of bulk aerosol) and mass (74% of the total bulk aerosol mass) basis. Ammonium has a 5-year average concentration of 45.2 ± 42.2 (standard deviation, SD) nmol m^{-3}, a median concentration of 30.71 nmol m^{-3},

Table 1. NH_4^+ Concentration Statistics Sorted by Season and Year[a]

	Winter						Spring					
NH_4^+, %	2000	2001	2002	2003	2004	All	2000	2001	2002	2003	2004	All
N	45	65	78	79	86	**353**	64	82	89	83	89	**407**
5th	14.1	9.16	11.6	9.58	6.21	**10.1**	9.89	7.91	9.41	11.6	7.72	**9.31**
50th	36.3	34.4	35.5	27.1	17.7	**30.2**	27.3	25.1	31.1	31.9	33.2	**29.7**
95th	123	96.6	114	102	87.2	**105**	86.2	85.6	104	91.0	111	**89.6**
	Summer						Fall					
NH_4^+, %	2000	2001	2002	2003	2004	All	2000	2001	2002	2003	2004	All
N	84	73	84	92	86	**419**	90	65	91	87	59	**392**
5th	8.23	9.94	5.13	8.56	14.5	**9.27**	6.60	8.29	7.32	7.17	10.4	**7.96**
50th	34.7	42.9	34.4	38.5	55.9	**41.3**	25.6	30.4	23.4	24.5	33.3	**27.4**
95th	133	192	205	158	239	**181**	106	110	105	90.6	106	**104**

[a]All units are nmol m^{-3}. To convert to ng m^{-3}, multiply by 18. Five-year averaged seasonal data are in bold for comparison. N is the number of samples in each season and year. Seasons are defined as follows: Winter is December, January, February; spring is March, April, May; summer is June, July, August; and fall is September, October, November. January defines the winter year.

and a range from below detection limit to 353 nmol m^{-3}. Sulfate has a 5-year average concentration of 26.2 ± 24.8 (SD) nmol m^{-3}, a median concentration of 18.1 nmol m^{-3}, and a range from below detection limit to 198 nmol m^{-3}. The considerable difference between the average and median for both species indicates that the averages are influenced heavily by large spikes in concentration. The episodic nature of high aerosol concentration events is evident in Figure 2. Inferred fine mode NO_3^- has a 5-year average concentration of 2.0 nmol m^{-3}, a median concentration below the uncertainty value, and a maximum measured concentration of 91.9 nmol m^{-3}, all considerably lower than $[NH_4^+]$ and $[SO_4^{2-}]$. Because fine mode NO_3^- is a calculated quantity, the uncertainty (again, defined as three times the standard deviation of duplicates and blanks) is used instead of the measurement detection limit. Concentrations for calculated fine mode NO_3^- are below the measurement uncertainty for over 67% of sampled days, while $[NH_4^+]$ and $[SO_4^{2-}]$ are below detection limits for less than 1% of sampled days. Overall, the calculated average $[NO_3^-]$ in the coarse mode is over four times greater than the average $[NO_3^-]$ in the fine mode.

[29] A strong seasonality is observed in the continuous daily concentration time series for NH_4^+, NO_3^-, and SO_4^{2-}. Monthly statistics for each species are summarized in Figures 2b, 2d, and 2f. Sulfate peaks during the summer months at TF and is at a minimum during the fall and winter. While monthly median values vary from 12 nmol m^{-3} in November to 28 nmol m^{-3} in August, 95th percentile values range by over a factor of three, from 40 nmol m^{-3} in November to 130 nmol m^{-3} in August. More variability in $[SO_4^{2-}]$ is observed during the summer compared to the winter, as illustrated by a higher ratio of the standard deviation to the median during August compared to during November (1.6 compared to 0.77). Higher summertime temperatures and increased photochemistry provide elevated OH, O_3, and H_2O_2 concentrations, resulting in increased SO_4^{2-} production.

[30] Ammonium concentrations track $[SO_4^{2-}]$, as is indicated by Figure 3 that shows a regression between $[NH_4^+]$ and $[SO_4^{2-}]$ with good correlation (R^2 = 0.94). This high temporal correlation between NH_4^+ and SO_4^{2-} is expected given that NH_4^+ is the major base available to neutralize sulfuric acid aerosol and that NH_4HSO_4 and $(NH_4)_2SO_4$, the products of neutralization, are very stable in the aerosol phase at atmospherically relevant temperatures and pressures [*Charlson et al.*, 1978]. The ratio of $[NH_4^+]$ to $[SO_4^{2-}]$ is similar in nature to *f* and is approximately 1.6 on average on the basis of the regression shown in Figure 3. This is consistent with slightly acidic aerosols.

[31] The calculated time series and monthly statistics for aerosol acidity and acid purity are presented in Figure 4.

Table 2. NO_3^- Concentration Statistics Sorted by Season and Year[a]

	Winter						Spring					
NO_3^-, %	2000	2001	2002	2003	2004	All	2000	2001	2002	2003	2004	All
N	45	65	78	79	86	**353**	64	82	89	83	89	**407**
5th	0.00	0.00	0.00	0.00	0.00	**0.00**	0.00	0.00	0.00	0.00	0.00	**0.00**
50th	0.00	0.00	0.98	0.00	0.00	**0.20**	0.00	0.00	0.00	0.00	0.00	**0.00**
95th	19.5	9.32	42.8	11.6	6.87	**18.1**	4.57	5.98	5.60	2.47	2.18	**4.16**
	Summer						Fall					
NO_3^-, %	2000	2001	2002	2003	2004	All	2000	2001	2002	2003	2004	All
N	84	73	84	92	86	**419**	90	65	91	87	59	**392**
5th	0.00	0.00	0.00	0.00	0.00	**0.00**	0.00	0.00	0.00	0.00	0.00	**0.00**
50th	0.00	0.00	0.00	0.00	0.00	**0.00**	0.07	0.31	0.00	0.00	0.00	**0.08**
95th	3.83	4.65	3.73	1.89	0.89	**3.75**	8.83	13.2	9.19	7.35	6.22	**8.96**

[a]All units are nmol m^{-3}. To convert to ng m^{-3}, multiply by 62. N is the number of samples in each season and year. Five-year averaged seasonal data are in bold for comparison. Seasons are defined in the Table 1 caption.

Table 3. SO_4^{2-} Concentration Statistics Sorted by Season and Year[a]

	Winter						Spring					
SO_4^{2-}, %	2000	2001	2002	2003	2004	All	2000	2001	2002	2003	2004	All
N	45	65	78	79	86	**353**	64	82	89	83	89	**407**
5th	8.65	4.79	6.30	6.19	3.75	**5.94**	5.70	8.17	5.50	6.47	8.36	**6.84**
50th	20.1	20.6	18.5	14.3	11.8	**17.1**	16.8	19.2	19.3	19.0	21.3	**19.1**
95th	49.1	48.1	45.4	59.6	37.7	**48.0**	49.6	57.8	59.1	49.3	58.8	**54.9**
	Summer						Fall					
SO_4^{2-}, %	2000	2001	2002	2003	2004	All	2000	2001	2002	2003	2004	All
N	84	73	84	92	86	**419**	90	65	91	87	59	**392**
5th	3.65	5.76	2.76	4.92	6.56	**4.73**	2.96	4.72	4.64	3.94	4.67	**4.19**
50th	20.5	25.1	19.4	23.5	30.1	**23.7**	12.9	16.8	13.4	14.6	18.1	**15.2**
95th	74.7	106	101	98.5	156	**107**	64.4	73.7	60.0	54.5	71.1	**64.7**

[a]All units are nmol m^{-3}. To convert to ng m^{-3}, multiply by 96. N is the number of samples in each season and year. Five-year averaged seasonal data are in bold for comparison. Seasons are defined in the Table 1 caption.

Seasonal and yearly statistics for inferred $[H^+]$ are presented in Table 4. The estimated acidity of aerosols sampled at TF is highly variable, as $[H^+]$ ranged from zero to 281 nmol m^{-3} (off the scale of Figure 4) and exhibited high day-to-day variability (standard deviation of 15.8 nmol m^{-3}). Maximum concentrations are calculated in early spring (March and April) and late summer (August). Minimum $[H^+]$ is calculated during November. Median monthly inferred $[H^+]$ ranges from 8 nmol m^{-3} in August to 2 nmol m^{-3} in December. Monthly peaks for measured $[SO_4^{2-}]$ and inferred $[H^+]$ in the summer agree qualitatively with previous longer-term measurements and calculations of this type [*Malm et al.*, 2002, 2004].

[32] Most of the day-to-day variability (over a month-long period) in calculated $[H^+]$ (defined as the ratio of the 95th percentile and median values for inferred $[H^+]$) is observed in July and August (10 and 9.6 for July and August, respectively) compared to very little variability (ratio of 3.7) in November. A clear minimum in median inferred $[H^+]$ is found during the fall and winter, especially November and December (3.1 and 2.2 nmol m^{-3}, respectively), which coincides with minimum $[SO_4^{2-}]$ during these months (14 and 15 nmol m^{-3}, respectively). A seasonal increase in inferred $[H^+]$ during March and April seems to be weighted heavily by high 95th percentile $[NO_3^-]$ during the spring of 2001 and the lowest median $[NH_4^+]$ measured at TF during any spring season (25.1 nmol m^{-3}, 15% lower than the 5-year median). However, the decrease in median calculated $[H^+]$ during May and June (23 and 36% below values for April) is likely associated with the application of fertilizers either near the sampling site or at some point upwind. No NH_3 emission data is available for this area and study period, but modeling results suggest that NH_3 emissions are much greater during the summer than during the winter [*Gilliland et al.*, 2003].

[33] In contrast, the day-to-day variability in calculated acid purity is highest during November and December (4.4 and 4.7, respectively) and smallest during July and August (2.8 for both). The time series shows high day-to-day variability and values covering the zero to unity scale. The majority (over 97%) of samples have values below 0.5 (shown in Figure 4). As a ratio, acid purity is less sensitive to changes in ionic concentrations than is $[H^+]$, illustrated by the larger variability in $[H^+]$ compared to acid purity.

3.2. Size-Segregated Aerosol Chemical Compositions

[34] Data from the VAPS (shown in Figure 5) confirmed that SO_4^{2-} and NH_4^+ constituted the majority of inorganic chemical constituents of fine aerosol, 96% by mass, while NO_3^- contributed negligibly (1.4%) during summer. Most of the remaining inorganic mass was composed of Na^+, likely from intrusions of sea-salt aerosol into the fine mode. The lack of significant fine $[NO_3^-]$ is consistent with low $[NO_3^-]$ during the summer calculated from the Cl^- depletion method for the bulk filters.

[35] At TF during ICARTT, the mass of coarse aerosol is almost an order of magnitude smaller than the fine aerosol mass and is dominated by NO_3^-, Na^+, and Cl^- (89% by mass on average; data not shown). An average of 88% (by gravimetric analysis) of PM_{10} is in the fine aerosol mode. Highest masses in the coarse mode are associated with backward trajectories originating over oceanic or coastal regions. The average ratio of Mg^{2+} to Na^+ for all coarse samples is 0.129, consistent with a ratio of 0.121 predicted from bulk seawater. Only two out of a total 18 coarse mode samples contain SO_4^{2-} above detection limits. All (> 99.9%)

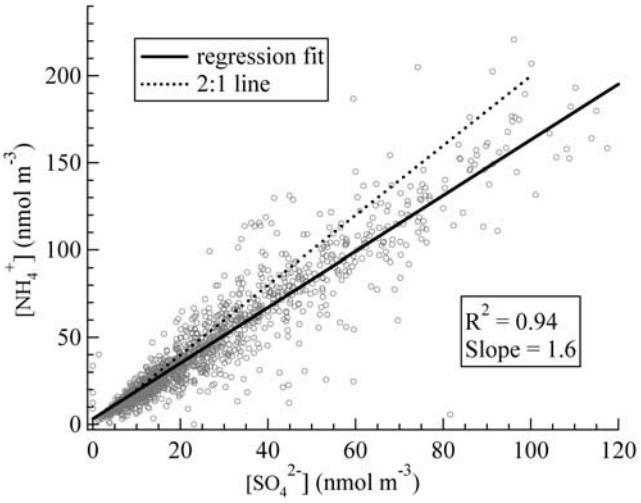

Figure 3. Regression between $[NH_4^+]$ and $[SO_4^{2-}]$.

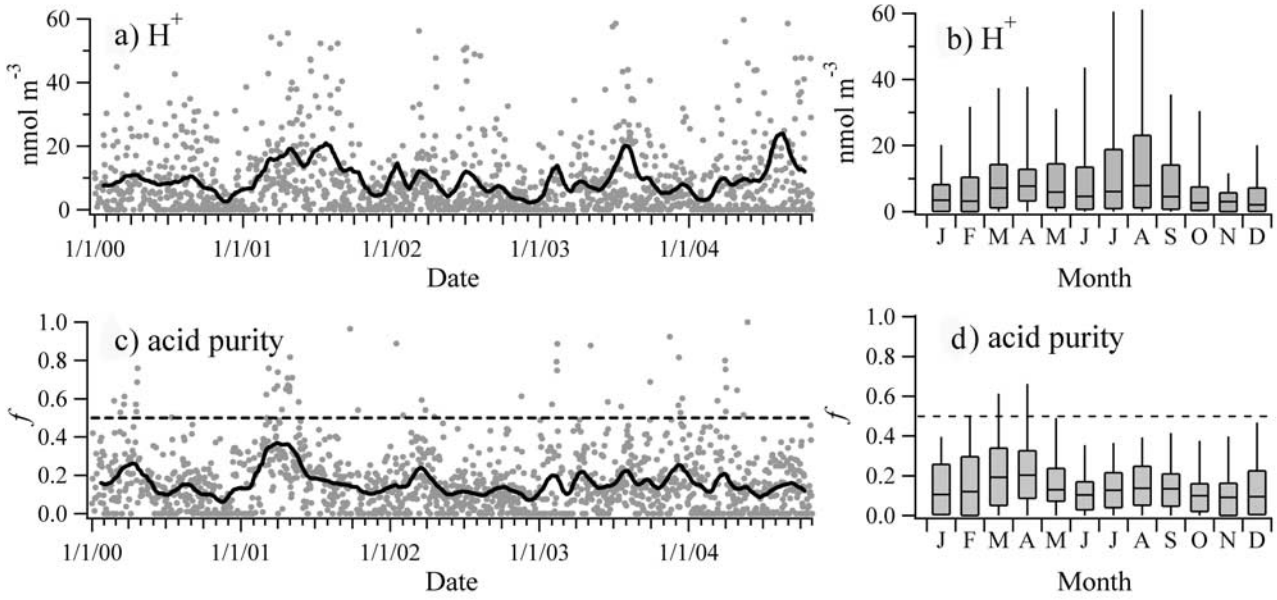

Figure 4. Time series and box plot analyses for (a and b) H^+ and (c and d) acid purity. A 30-day running average has been applied to each time series plot and is shown as a bold line. Box plot configuration is defined as in the caption for Figure 1. A dashed line has been added to Figures 4c and 4d at $f = 0.5$ to represent 50% neutralization.

of the measured coarse mode NO_3^- exists because of displacement reactions, as the amount predicted to be from sea salt by NO_3^- to Na^+ and NO_3^- to Mg^{2+} ratios is extremely low. This is very consistent with the previously described method for size segregation of NO_3^- from the bulk filter analysis.

[36] Comparison of mass concentrations by gravimetric and chemical analysis results in a correlation coefficient of 0.92 and a slope of 0.81. The reconstructed chemical composition mass is a simple summation of the mass of all species measured. Discrepancies exist on days of very high mass loading and may be explained by negative artifacts associated with filter sampling of organic species [*Subramanian et al.*, 2004], significant mass due to particle water or other unidentified species, or underestimation of the OM/OC ratio. Approximately 20% of measured aerosol organic carbon in Atlanta, GA, was identified to be of acidic nature [*Sullivan and Weber*, 2006]. Given this fraction, the relatively weak nature of organic acids relative to H_2SO_4 and HNO_3, and the fact that it is not known a priori if these acids in fact resided in the aqueous phase, it is assumed in this study that organics do not contribute significantly to acidity. In this case, gravimetric analysis shows that chemical analyses have sufficiently accounted for the majority of aerosol mass related to inference of $[H^+]$.

3.3. Source Region Analysis

[37] Back trajectories were sorted into six source regions representing different paths taken to TF (Figure 1). Fifty-five percent of the analyzed trajectories are classified as having a continental-Canadian source region, while 21% are classified as continental-midwestern. Other source regions are observed far less frequently: 9% from the marine-Canadian region, 8% from the marine-coastal region, 5% from the continental-coastal region, and 3% from the marine

Table 4. Calculated H^+ Concentration Statistics Sorted by Season and Year[a]

	Winter						Spring					
H^+, %	2000	2001	2002	2003	2004	All	2000	2001	2002	2003	2004	All
N	45	65	78	79	86	**353**	64	82	89	83	89	**407**
5th	0.00	0.00	0.00	0.00	0.00	**0.00**	0.02	3.31	0.00	0.00	0.00	**0.66**
50th	6.18	3.06	4.45	0.99	2.15	**3.37**	6.22	14.1	6.07	6.06	4.84	**7.46**
95th	24.8	24.0	15.8	30.5	20.1	**23.0**	27.4	52.1	27.0	20.6	37.2	**32.9**
	Summer						Fall					
H^+, %	2000	2001	2002	2003	2004	All	2000	2001	2002	2003	2004	All
N	84	73	84	92	86	**419**	90	65	91	87	59	**392**
5th	0.00	0.17	0.00	0.00	0.00	**0.03**	0.00	0.00	0.00	0.00	0.00	**0.00**
50th	5.03	8.60	2.78	8.82	7.66	**6.58**	1.74	4.56	3.55	4.26	4.32	**3.69**
95th	29.0	52.3	46.8	50.1	71.2	**49.9**	25.3	26.5	20.2	20.7	42.1	**27.0**

[a]All units are nmol m^{-3}. N is the number of samples in each season and year. Five-year averaged seasonal data are in bold for comparison. Seasons are defined in the Table 1 caption.

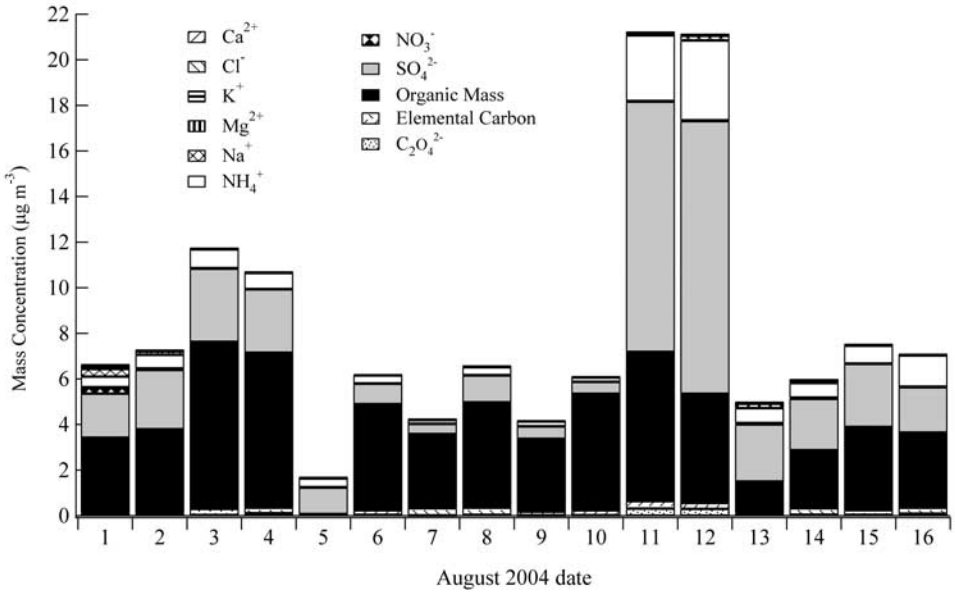

Figure 5. Aerosol fine mode chemical composition as measured using the VAPS at TF during ICARTT. No organic mass or elemental carbon data are available for 5 August 2004.

region. This source distribution is considered "normal" for all trajectories computed during this analysis. Source regions as a function of aerosol chemistry are all compared to this normal distribution to assess the dependence of chemical composition of aerosol on transport.

[38] The source distribution for each season and for all data is reported in Figure 6. Few differences in source regions are found seasonally, with the only significant difference being an increase in continental-Canadian sources during the winter months. Source regions for varying aerosol chemistry are compared to normal and are illustrated in Figure 7. Continental-coastal, midwestern, and marine-coastal source regions are 6, 8, and 8% increased (compared to the normal distribution), respectively, for 75th–95th percentile inferred $[H^+]$ samples, and the same source regions are increased by 8, 9, and 13%, respectively, for samples with $[H^+]$ greater than the 95th percentile. Lowest inferred $[H^+]$ and *f* values are associated with the continental-Canada region, as are lowest observed $[SO_4^{2-}]$. The trend observed for high acid purity samples differs slightly, as there is less influence from midwestern sources. Greater than 75th percentile *f* is 17% more likely to be of marine or coastal influence (the total of continental-coastal, marine-coastal, marine-Canadian, and marine) and is 8 and 10% less likely to be originating from the continental-Canadian and midwestern source regions, respectively. High $[NO_3^-]$ events are almost exclusively associated with increased continental-midwestern flow regimes (by 18%) while high $[SO_4^{2-}]$ appears with large increases in continental-midwestern

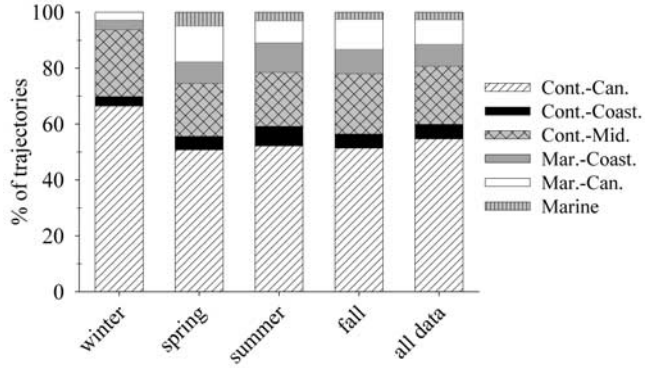

Figure 6. Source region distribution of air masses reaching TF, sorted by season. The source distribution for all of the data is also presented. Seasons are defined in the caption of Table 1. Only days that met the 2/3 criteria described in the text were included in this analysis.

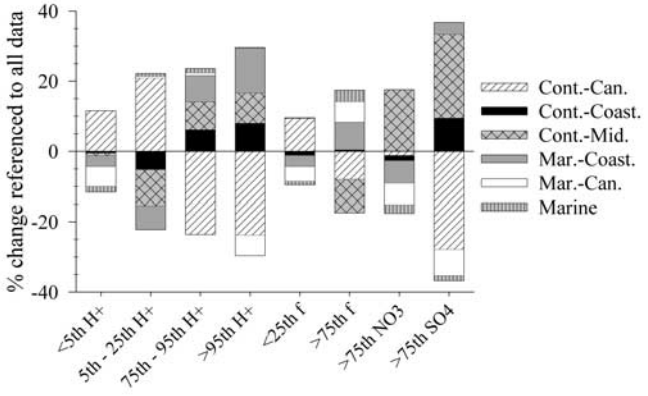

Figure 7. Change in source distribution for aerosol of varying chemical composition. Percentiles on *x* axis refer to all data. Percent change on *y* axis refers to a source distribution change relative to the source distribution for all data (shown in Figure 6).

(24%) and both coastal source regions (a 10% total when the changes are summed).

4. Discussion

4.1. Year-to-Year Variability

[39] Although backward trajectory analyses yield few differences in overall source regions on a seasonal basis, considerable year-to-year variability in aerosol concentrations is observed. Seasonal and yearly statistics for $[NH_4^+]$, $[NO_3^-]$, $[SO_4^{2-}]$, and $[H^+]$ are presented in Tables 1–4 to highlight this variability. For this discussion, the median $[SO_4^{2-}]$ values shown in Table 3 are considered. A high value for the maximum to minimum median concentration ratio for a given season and species indicates more year-to-year variability, and a value of 1.0 for this ratio would indicate no variability. Year-to-year variability is largest for $[SO_4^{2-}]$ during winter (1.75), smaller during the summer (1.63), and smallest during the spring and fall seasons (1.27 and 1.40, respectively). This trend is analogous to the year-to-year variability in $[NH_4^+]$.

[40] Given that winter and summer exhibit the greatest interannual variability, minimum and maximum years for these seasons for NH_4^+ and SO_4^{2-} were considered. For both species, the summer with the lowest median concentrations is 2002 and that with the highest was 2004. Compared to the median concentrations for all summer data, summer 2002 was 16.7% lower than average for NH_4^+ and 18.1% lower than average for SO_4^{2-}. Conversely, during summer of 2004, higher than average concentrations of these ions were measured, with increases of 35.4% and 27.0%, respectively. No relationship between these anomalies and average temperature or precipitation extremes could be identified. It should be stressed, however, that a more in-depth analysis of climate variability during the study period would be necessary to better elucidate a potential relationship between climate and aerosol concentrations and characteristics.

[41] Unquestionably, the season of largest calculated aerosol acidity is the spring of 2001, as shown in Table 4. This season is described by the greatest 5th percentile concentration of any season (essentially the only significant 5th percentile above a zero level), the greatest median value of any season by almost a factor of two, and the third greatest 95th percentile value. While the inferred $[H^+]$ for this season is unique for the spring, it is on par with the largest acid concentrations estimated for the typically more polluted summer. The spring of 2001 season is also marked by one of the smallest $[NH_4^+]$, especially for the spring, and the greatest $[NO_3^-]$ of any spring. The largest spring season $[NO_3^-]$ recorded on Mount Washington (MW, 44.27°N, 71.30°W, and 1,917 m above sea level) coincides with the high $[NO_3^-]$ at TF during the spring of 2001 [*Fischer et al.*, 2007]. Interestingly, *Schwab et al.* [2004] report no concurrent increase in acidity during this month at any of their sites in upstate New York. This season is actually one of the seasons with the smallest estimated $[H^+]$ in their data set.

[42] *DeBell et al.* [2004] report the extensive regional influence of Asian dust storm events from 18 April 2001 through 13 May 2001; such dust storms import entrained NO_3^- and HNO_3 that potentially affect the acidity calculation. However, given the coastal path taken by air masses during the dust events, concurrent $[H^+]$ increases may not have been observed at the rural site in New York. Anomalously large inferred acid concentrations may also indicate that methods used in this study were less applicable during this time period.

4.2. Source Region Control on *f* and H^+

[43] General transport characteristics at TF are consistent with the results of *Fischer et al.* [2007] for MW, although differing analysis techniques were used. The source distributions at both TF (based on backward trajectory analysis) and MW (based on measured wind direction) are dominated by westerly and northwesterly flows. Both analyses showed very little seasonal change in source distribution, with the exception of increased northwestern flow in the winter. High $[SO_4^{2-}]$ at both TF and MW is attributed to increases in southwesterly flow.

[44] Our analysis suggests that highly populated metropolitan areas such as Boston, Massachusetts, New York City, New York, and Washington, DC, may be important sources of aerosol with high acidity. While aerosol with large inferred $[H^+]$ originates from polluted areas, aerosol that was less neutralized originates over coastal and marine regions. We hypothesize that this was the result of less air mass interaction with NH_3 along these trajectories. To the authors' knowledge, this air mass source dependence of $[H^+]$ compared to *f* has not been observed previously.

4.3. Nitrate Aerosol in Winter Versus Summer

[45] The stability exhibited by neutralized particulate SO_4^{2-} is not applicable to NO_3^-, which is considerably more volatile in ambient aerosol [*Tang*, 1980]. Fine $[NO_3^-]$ is generally an order of magnitude smaller than $[SO_4^{2-}]$ at this site because of insufficient NH_4^+, relatively high temperatures that favor partitioning to the gas phase, and probable source strength differences between SO_2 and NO_x [*Tang*, 1980; *Seinfeld and Pandis*, 1998]. Nitrate concentrations peak during the colder winter months (Figure 2). This trend is evident in the variability in 95th percentile values for NO_3^-, which range from 2.5 nmol m^{-3} in August to 40 nmol m^{-3} in January. As temperatures increase, the combined effect of increasing $[SO_4^{2-}]$ to associate with NH_3 and increasing volatility of nitrate species inhibits the formation of aerosol phase NO_3^-, resulting in summertime minima.

[46] While aerosol phase NO_3^- and SO_4^{2-} result primarily from the reaction of their precursors with photochemically derived species, the differing seasonal trends also can be explained partially by a greater sensitivity of NO_3^- formation to changing temperature, both thermodynamically and kinetically. First, the vapor pressure of HNO_3 decreases by a factor of 75 as the temperature decreases from 310 K to 240 K. Second, the equilibrium constant for the reversible reaction of $NH_{3(g)}$ and $HNO_{3(g)}$ to form $NH_4NO_{3(s)}$ increases by eight orders of magnitude as temperature decreases from 310 K to 240 K [*Stelson and Seinfeld*, 1982], highly favoring the production of particulate NH_4NO_3 during the winter. Reaction kinetics play a smaller but similar role in the winter NO_3^- peak. The calculated effective second-order reaction rate constant for the formation of HNO_3 from the NO_2-OH reaction increases by

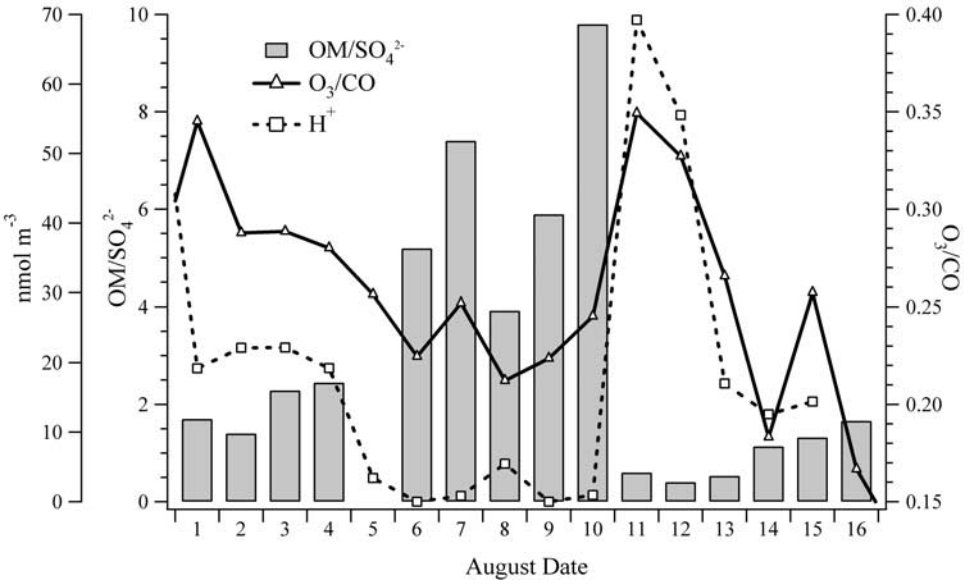

Figure 8. Ratio of OM to $[SO_4^{2-}]$ determined from VAPS filters, the ratio of O_3 to CO determined from data provided by the AIRMAP monitoring network, and the relative acidity of fine aerosols determined from VAPS filters using equation (1).

43.3% as the temperature decreases from 310 K to 240 K [*DeMore et al.*, 1994]. The ratio of the rate constants for reactions of NO_2 and SO_2 with OH $[(k_{NO2\text{-}OH})/(k_{SO2\text{-}OH})]$ increases by 26.5% over the same temperature range, indicating that gas phase NO_3^- reaction kinetics are more sensitive than SO_4^{2-} reaction kinetics to temperature change. These conditions combine to favor formation of NH_4NO_3 when NH_3 emissions increase during warm winter periods [*Fischer and Talbot*, 2005].

4.4. Relationship Between OM, Sulfate, and Photochemical Age

[47] The ratio of OM to SO_4^{2-} has been computed to assess the relative influence of biogenic and anthropogenic sources for each sample and to compare this to the inferred $[H^+]$ for the VAPS samples. While large values of the ratio of OM to SO_4^{2-} indicate a stronger relative biogenic influence, small values are indicative of stronger relative anthropogenic influences [*Venkataraman et al.*, 2002]. However, this ratio should not be used to imply that either biogenic or anthropogenic emissions cease to be important at any time. From 10-min averages from an aerosol mass spectrometer, this ratio varies from 0.25 to 41.4, with an average of 4.3, at TF during ICARTT (L. D. Cottrell et al., Submicron particles at Thompson Farm during ICARTT measured using aerosol mass spectrometry: Case studies of organic and sulfate aerosol, manuscript in preparation, 2007). The O_3 to carbon monoxide (CO) ratio is a metric to indicate the degree of photochemical aging to which an air mass has been subjected prior to arrival at TF [*Fishman and Seiler*, 1983], with values approaching 0.37 indicating a high degree of photochemical aging for TF in summer [*Griffin et al.*, 2004; *Mao and Talbot*, 2004a]. Inferred $[H^+]$, the OM to SO_4^{2-} ratio, and the ratio of O_3 to CO are plotted in Figure 8 for all 24-hour ICARTT VAPS filters. Daytime (defined here as 1000–1700 local time) averaged O_3 and CO concentrations are used in the O_3 to CO ratio to control for the diurnal character of O_3 at TF. While the OM/OC ratio is likely to vary considerably depending on the functionality of organic compounds in aerosol, the conclusions made here based on the temporal behavior of the relative OM to SO_4^{2-} ratios would be insensitive to changes in the OM/OC ratio used.

[48] It is evident that high inferred acid concentrations (69 and 56 nmol m^{-3}) on 11 and 12 August 2004 are coincident with a decrease in the ratio of OM to SO_4^{2-} (0.6 and 0.4, respectively) and an increase in the ratio of O_3 to CO (0.35 and 0.33, respectively), implying that this acidic air mass is more anthropogenic and more photochemically aged. Backward trajectories show that on 11 and 12 August 2004, air masses originated from coastal and midwestern source regions. On the other hand, aerosol sampled on 6–10 August 2004 lacks significant inferred $[H^+]$ (1.7 nmol m^{-3} average) and is associated with increased values of the OM to SO_4^{2-} ratio (6.4 average) and decreased values of the O_3 to CO ratio (0.23 average), implying a stronger biogenic influence and less photochemical aging. For the 6–10 August 2004 period, surface winds were exclusively from northwesterly directions, and backward trajectories confirmed a dominant Canadian source region. Aerosol acidity is well correlated (R^2 = 0.76) with the ratio of O_3 to CO throughout this period. This is evidence that regional transport and aging likely play integral roles in controlling aerosol acidity at this site.

4.5. Relationship Between OM and H^+

[49] To investigate the relationship between aerosol acidity and increased SOA, a comparison was made between [OM] and inferred $[H^+]$. No significant correlation (R^2 = 0.38) exists between particle acidity and increased total [OM], contrary to experimental work from *Jang et al.* [2002] and *Iinuma et al.* [2004] and to field observations in power plant plumes by *Brock et al.* [2003]. Large [OM] exist during transport from not only the southeast but also

the northwest, potentially indicating the influence of biogenic SOA that formed without acid catalysis. A similar lack of correlation between acidity and SOA formation was reported by *Takahama et al.* [2006] during the Pittsburgh Air Quality Study using a scatterplot/wind direction analysis technique. It is important to note that the ICARTT data set is restricted to 3 weeks of filter samples and TF may not represent an ideal site for assessing SOA acid catalysis.

5. Conclusions

[50] The majority of fine ionic aerosol mass at TF, a site thought to be representative of semirural northern New England, is composed primarily of SO_4^{2-} and NH_4. Particulate SO_4^{2-} is driven strongly by photochemical seasonality. Fine particulate NO_3^- makes a minor contribution to the overall inorganic mass and is highly dependent on lower temperatures that inhibit volatilization, increase formation reaction rates, and shift chemical equilibrium toward NH_4NO_3.

[51] Temporal analyses show a clear seasonal variation of the three major species that influence fine aerosol acidity at TF. The seasonal trends in aerosol acidity, however, are more convoluted because they are affected by all three ionic species. Seasonal patterns generally follow the seasonality associated with SO_4^{2-}. Acid purity, or the extent of neutralization of the aerosol, however, tends to be less episodic throughout all seasons. Aerosols with high inferred acidity during ICARTT are associated with anthropogenically influenced, well aged air masses, as indicated by low values of the OM to SO_4^{2-} ratio and high values of the O_3 to CO ratio.

[52] While variations in seasonal transport cannot explain the observed differences in seasonal aerosol composition, differences in transport can explain day-to-day variability in observed concentrations. Aerosols with high inferred $[H^+]$ are more frequent in coastal air masses that pass over major metropolitan areas along the eastern seaboard of the United States. This may result from both increased SO_2 and decreased NH_3 relative emissions in these areas. Transport from midwestern areas such as the Ohio River valley and the Great Lakes region are sources of increased $[SO_4^{2-}]$, $[NH_4^+]$, and inferred $[H^+]$. Although polluted air masses carry high inferred $[H^+]$, less neutralized aerosol arises from less polluted maritime sources with weaker NH_3 emissions.

[53] **Acknowledgments.** We gratefully acknowledge funding from the Office of Oceanic and Atmospheric Research of NOAA under AIRMAP grants NA03OAR4600122 and NA04OAR4600154. Any opinions, findings, conclusions and/or recommendations expressed in this material are those of the authors and do not necessarily reflect the views of the funding agency. The authors also gratefully acknowledge the NOAA Air Resources Laboratory for provision of the HYSPLIT model and READY website (http://www.arl.noaa.gov/ready.html) used in this publication. We would also like to thank Jack Dibb, Ruth Varner, and anonymous reviewers for helpful comments.

References

Birch, M. E., and R. A. Cary (1996), Elemental carbon-based method for monitoring occupational exposures to particulate diesel exhaust, *Aerosol Sci. Technol.*, *25*, 221–241.

Bluth, G. J. S., T. J. Casadevall, C. C. Schnetzler, S. D. Doiron, L. S. Walter, A. J. Krueger, and M. Badruddin (1994), Evaluation of sulfur-dioxide emissions from explosive volcanism—The 1982–1983 eruptions of Galunggung, Java, Indonesia, *J. Volcanol. Geotherm. Res.*, *63*, 243–256.

Botha, C. F., J. Hahn, J. J. Pienaar, and R. Van Eldik (1994), Kinetics and mechanism of the oxidation of sulfur(IV) by ozone in aqueous solutions, *Atmos. Environ.*, *20*, 3207–3212.

Bouwman, A. F., D. S. Lee, A. H. Asman, F. J. Dentener, K. W. Van Der Hoek, and J. G. J. Olivier (1997), A global high-resolution emission inventory for ammonia, *Global Biogeochem. Cycles*, *11*, 561–587.

Brock, C. A., et al. (2003), Particle growth in urban and industrial plumes in Texas, *J. Geophys. Res.*, *108*(D3), 4111, doi:10.1029/2002JD002746.

Brosset, C. (1978), Water-soluble sulfur compounds in aerosol, *Atmos. Environ.*, *12*, 25–38.

Charlson, R. J., D. S. Covert, T. V. Larson, and A. P. Waggoner (1978), Chemical properties of tropospheric sulfur aerosol, *Atmos. Environ.*, *12*, 39–53.

Charlson, R. J., T. L. Anderson, and R. E. McDuff (1992a), The sulfur cycle, in *Global Biogeochemical Cycles*, edited by S. S. Butcher et al., pp. 285–300, Elsevier, New York.

Charlson, R. J., S. E. Schwartz, J. M. Hales, R. D. Cess, J. A. J. Coakley, J. E. Hansen, and D. J. Hofmann (1992b), Climate forcing by anthropogenic aerosols, *Science*, *255*, 423–430.

DeBell, L. J., M. Vozzella, R. W. Talbot, and J. E. Dibb (2004), Asian dust storm events of spring 2001 and associated pollutants observed in New England by the Atmospheric Investigation, Regional, Modeling, Analysis and Prediction (AIRMAP), monitoring network, *J. Geophys. Res.*, *109*, D01304, doi:10.1029/2003JD003733.

DeMore, W. G., S. P. Sander, D. M. Golden, R. F. Hampson, M. J. Kurylo, C. J. Howard, A. R. Ravishankara, C. E. Kolb, and M. J. Molina (1994), Chemical kinetics and photochemical data for use in stratospheric modeling, evaluation 11, *JPL Publ. 94-26,* Jet Propul. Lab., Pasadena, Calif.

Draxler, R. R., and G. D. Rolph (2003), HYSPLIT (Hybrid Single-Aerosol Lagrangian Integrated Trajectory), model access via NOAA ARL READY Web site, Air Resour. Lab., NOAA, Silver Spring, Md. (Available at http://www.arl.noaa.gov/ready/hysplit4.html)

Dzubay, T. G., R. K. Stevens, C. W. Lewis, D. H. Hern, J. W. Courtney, J. W. Tesch, and M. A. Mason (1982), Visibility and aerosol composition in Houston, Texas, *Environ. Sci. Technol.*, *16*, 514–525.

Fehsenfeld, F. C., et al. (2006), International Consortium for Atmospheric Research on Transport and Transformation (ICARTT): North America to Europe—Overview of the 2004 summer field study, *J. Geophys. Res.*, *111*, D23S01, doi:10.1029/2006JD007829.

Fischer, E., and R. Talbot (2005), Regional NO_3^- events in the northeastern United States related to seasonal climate anomalies, *Geophys. Res. Lett.*, *32*, L16804, doi:10.1029/2005GL023490.

Fischer, E. V., R. W. Talbot, J. E. Dibb, J. L. Moody, and G. L. Murray (2004), Summertime ozone at Mount Washington: Meteorological controls at the highest peak in the northeast, *J. Geophys. Res.*, *109*, D24303, doi:10.1029/2004JD004841.

Fischer, E. V., L. D. Ziemba, R. W. Talbot, J. E. Dibb, R. J. Griffin, L. Husain, and A. N. Grant (2007), Aerosol major ion record at Mount Washington, *J. Geophys. Res.*, *112*, D02303, doi:10.1029/2006JD007253.

Fishman, J., and W. Seiler (1983), Correlative nature of ozone and CO in the troposphere: Implications for the tropospheric ozone budget, *J. Geophys. Res.*, *88*, 3663–3670.

Fitzgerald, J. W. (1991), Marine aerosol—A review, *Atmos. Environ.*, *25*, 533–545.

Gard, E. E., et al. (1998), Direct observation of heterogeneous chemistry in the atmosphere, *Science*, *279*, 1184–1187.

Gilliland, A. B., R. L. Dennis, S. J. Roselle, and T. E. Pierce (2003), Seasonal NH_3 emission estimates for the eastern United States based on ammonium wet concentrations and an inverse modeling method, *J. Geophys. Res.*, *108*(D15), 4477, doi:10.1029/2002JD003063.

Griffin, R. J., C. A. Johnson, R. W. Talbot, H. Mao, R. S. Russo, Y. Zhou, and B. C. Sive (2004), Quantification of ozone formation metrics at Thompson Farm during the New England Air Quality Study (NEAQS) 2002, *J. Geophys. Res.*, *109*, D24302, doi:10.1029/2004JD005344.

Huntzicker, J. J., R. A. Cary, and C.-S. Ling (1980), Neutralization of sulfuric acid aerosol by ammonia, *Environ. Sci. Technol.*, *14*, 819–824.

Iinuma, Y., O. Boge, T. Gnauk, and H. Herrmann (2004), Aerosol-chamber study of the α-pinene/ozone reaction: influence of aerosol acidity on aerosol yields and products, *Atmos. Environ.*, *38*, 761–773.

Jang, M., N. M. Czoschke, S. Lee, and R. M. Kamens (2002), Heterogeneous atmospheric aerosol production by acid-catalyzed aerosol-phase reactions, *Science*, *298*, 814–817.

Jordan, C. E., R. W. Talbot, and B. D. Keim (2000), Water-soluble nitrogen at the New Hampshire sea coast: HNO_3, aerosols, precipitation, and fog, *J. Geophys. Res.*, *105*, 26,403–26,431.

Keeler, G. J., J. D. Spengler, P. Koutrakis, and G. A. Allen (1990), Transported acid aerosol measured in southern Ontario, *Atmos. Environ., Part A*, *24*, 2935–2950.

Keene, W. C., A. A. P. Pszenny, J. R. Maben, E. Stevenson, and A. Wall (2004), Closure evaluation of size-resolved aerosol pH in the New England coastal atmosphere during summer, *J. Geophys. Res.*, *109*, D23307, doi:10.1029/2004JD004801.

Kerminen, V.-M., R. Hillamo, K. Teinila, T. Pakkanen, I. Allegrini, and R. Sparapani (2001), Ion balances of size-resolved tropospheric aerosol samples: Implications for the acidity and atmospheric processing of aerosol, *Atmos. Environ.*, *35*, 5255–5265.

Knapp, K. G., B. B. Baisley, M. L. Jensen, H. P. Hanson, and J. W. Birks (1998), Observation of the transport of polluted air masses from the northeastern United States to Cape Sable Island, Nova Scotia, Canada, during the 1993 NARE summer intensive, *J. Geophys. Res.*, *103*, 13,399–13,411.

Koutrakis, P., J. M. Wolfson, and J. D. Spengler (1988), An improved method for measuring aerosol strong acidity—Results from a 9-month study in St. Louis, Missouri and Kingston, Tennessee, *Atmos. Environ.*, *22*, 157–162.

Kunen, S. M., A. L. Lazrus, G. L. Kok, and B. G. Heikes (1983), Aqueous oxidation of SO_2 by hydrogen peroxide, *J. Geophys. Res.*, *88*, 3671–3674.

Lefer, B. L., and R. W. Talbot (2001), Summertime measurements of aerosol NO_3^- and NH_4^+ at a northeastern U. S. site, *J. Geophys. Res.*, *106*, 20,365–20,378.

Li-Jones, X., and J. M. Prospero (1998), Variations in the size distribution of non-sea-salt sulfate aerosol in the marine boundary layer at Barbados: Impact of African dust, *J. Geophys. Res.*, *103*, 16,073–16,084.

Malm, W. C., B. A. Schichtel, R. B. Ames, and K. A. Gebhart (2002), A 10-year spatial and temporal trend of sulfate across the United States, *J. Geophys. Res.*, *107*(D22), 4627, doi:10.1029/2002JD002107.

Malm, W. C., B. A. Schichtel, M. L. Pitchford, L. L. Ashbaugh, and R. A. Eldred (2004), Spatial trends in speciated fine aerosol concentration in the United States, *J. Geophys. Res.*, *109*, D03306, doi:10.1029/2003JD003739.

Mao, H., and R. W. Talbot (2004a), O_3 and CO in New England: Temporal variations and relationships, *J. Geophys. Res.*, *109*, D21304, doi:10.1029/2004JD004913.

Mao, H., and R. W. Talbot (2004b), Relationship of surface O_3 to large-scale circulation patterns during two recent winters, *Geophys. Res. Lett.*, *31*, L06108, doi:10.1029/2003GL018860.

McInnes, L. M., D. S. Covert, P. K. Quinn, and M. S. Germani (1994), Measurements of chloride depletion and sulfur enrichment in individual sea-salt aerosol collected from the remote marine boundary layer, *J. Geophys. Res.*, *99*, 8257–8268.

Newberg, J. T., B. M. Matthew, and C. Anastasio (2005), Chloride and bromide depletions in sea-salt aerosol over the northeastern Pacific Ocean, *J. Geophys. Res.*, *110*, D06209, doi:10.1029/2004JD005446.

Russell, L. M. (2003), Aerosol organic-mass-to-organic-carbon ratio measurements, *Environ. Sci. Technol.*, *37*, 2982–2987.

Savoie, D. L., and J. M. Prospero (1982), Aerosol size distribution of NO_3^- and SO_4^{2-} in the marine atmosphere, *Geophys. Res. Lett.*, *9*, 1207–1210.

Schlesinger, R. B., and F. Cassee (2003), Atmospheric secondary inorganic particulate matter: The toxicological perspective as a basis for health effects risk assessment, *Inhal. Toxicol.*, *15*, 197–235.

Schultz, M., R. Schmitt, K. Thomas, and A. Volz-Thomas (1998), Photochemical box modeling of long-range transport from North America to Tenerife during the North Atlantic Regional Experiment (NARE) 1993, *J. Geophys. Res.*, *103*, 13,477–13,488.

Schwab, J. J., H. D. Felton, and K. L. Demerjian (2004), Aerosol chemical composition in New York state from integrated filter samples: Urban/rural and seasonal contrasts, *J. Geophys. Res.*, *109*, D16S05, doi:10.1029/2003JD004078.

Seinfeld, J. H., and S. N. Pandis (1998), *Atmospheric Chemistry and Physics: From Air Pollution to Climate Change*, John Wiley, Hoboken, N. J.

Smith-Palmer, T., and B. R. Wentzell (1986), Ambient acid aerosol in rural Nova Scotia, *Water Air Soil Pollut.*, *30*, 837–843.

Spengler, J. D., M. Brauer, and P. Koutrakis (1990), Acid air and health, *Environ. Sci. Technol.*, *24*, 946–955.

Stelson, A. W., and J. H. Seinfeld (1982), Relative humidity and temperature dependence of the ammonium nitrate dissociation constant, *Atmos. Environ.*, *16*, 983–993.

Stevens, R. K., T. G. Dzubay, R. W. Shaw, W. A. McClenny, C. W. Lewis, and W. E. Wilson (1980), Characterization of the aerosol in the Great Smoky Mountains, *Environ. Sci. Technol.*, *14*, 1491–1498.

Stockwell, W. R., and J. G. Calvert (1983), The mechanism of the HO-SO_2 reaction, *Atmos. Environ.*, *17*, 2231–2235.

Subramanian, R., A. Y. Khlystov, J. C. Cabada, and A. L. Robinson (2004), Positive and negative artifacts in particulate organic carbon measurements with denuded and undenuded sampler configurations, *Aerosol Sci. Technol.*, *38*, 27–48.

Sullivan, A. P., and R. J. Weber (2006), Chemical characterization of the ambient organic aerosol soluble in water: 2. Isolation of acid, neutral, and basic fractions by modified size-exclusion chromatography, *J. Geophys. Res.*, *111*, D05315, doi:10.1029/2005JD006486.

Takahama, S., C. I. Davidson, and S. N. Pandis (2006), Semi-continuous measurements of organic carbon and acidity during the Pittsburgh Air Quality Study: Implications for acid-catalyzed organic aerosol formation, *Environ. Sci. Technol.*, *40*, 2191–2199.

Tang, I. N. (1980), On the equilibrium partial pressures of nitric acid and ammonia in the atmosphere, *Atmos. Environ.*, *14*, 819–828.

Tsai, C. J., and S. N. Perng (1998), Artifacts of ionic species for hi-vol PM_{10} and PM_{10} dichotomous samplers, *Atmos. Environ.*, *32*, 1605–1613.

Turpin, B. J., and H. J. Lim (2001), Species contributions to PM2.5 mass concentrations: Revisiting common assumptions for estimating organic mass, *Aerosol Sci. Technol.*, *35*, 602–610.

U.S. Environmental Protection Agency (1999), Determination of the strong acidity of atmospheric fine particles (<2.5 μm), *EPA-625/R-96/010a*, Cent. of the Environ. Res. Inf., Cincinnati, Ohio.

U.S. Environmental Protection Agency (2001), Air quality criteria for particulate matter (second external review draft), *EPA Rep. EPA 600/P-99/002a,b,2v*, Off. of Res. and Dev., Research Triangle Park, N. C.

Venkataraman, C., C. K. Reddy, S. Josson, and M. S. Reddy (2002), Aerosol size and chemical characteristics at Mumbai, India, during the Indoex-IFP, *Atmos. Environ.*, *36*, 1979–1991.

Waldman, J. M., P. J. Lioy, G. D. Thurston, and M. Lippmann (1990), Spatial and temporal patterns in summertime SO_4^{2-} aerosol acidity and neutralization within a metropolitan area, *Atmos. Environ., Part B*, *24*, 115–126.

Wall, S. M., W. John, and J. L. Ondo (1988), Measurement of aerosol size distributions for nitrate and major ionic species, *Atmos. Environ.*, *22*, 1649–1656.

Wu, P. M., and K. Okada (1994), The nature of coarse nitrate aerosol in the atmosphere—A single aerosol approach, *Atmos. Environ.*, *28*, 2053–2060.

Yu, X.-Y., T. Lee, B. Ayers, S. M. Kreidenweis, J. L. Collett Jr., and W. Malm (2005), Loss of fine particle ammonium from denuded nylon filters, *J. Air Waste Manage. Assoc.*, *55*, 1100–1110.

Yu, X.-Y., T. Lee, B. Ayers, S. M. Kreidenweis, W. Malm, and J. L. Collett Jr. (2006), Loss of fine particle ammonium from denuded nylon filters, *Atmos. Environ.*, *40*, 4797–4807.

E. Fischer, Department of Atmospheric Sciences, University of Washington, Seattle, WA 98195, USA.

R. J. Griffin, R. W. Talbot, and L. D. Ziemba, Institute for the Study of Earth, Oceans, and Space, Climate Change Research Center, University of New Hampshire, Durham, NH 03824, USA. (rob.griffin@unh.edu)